Applied Physics Letters ARTICLE scitation.org/journal/apl

Spin-dependent polaron transport in helical molecules

Cite as: Appl. Phys. Lett. **121**, 143505 (2022); doi: 10.1063/5.0109240
Submitted: 12 July 2022 · Accepted: 10 September 2022 ·
Published Online: 7 October 2022

M. Barroso,[1] J. Balduque,[2] F. Domínguez-Adame,[1] and E. Díaz[1,a)]

AFFILIATIONS

[1]GISC, Departamento de Física de Materiales, Universidad Complutense, E-28040 Madrid, Spain
[2]Departamento de Física Teórica de la Materia Condensada, Universidad Autónoma de Madrid, E-28049 Madrid, Spain

[a)]Author to whom correspondence should be addressed: elenadg@ucm.es

ABSTRACT

We study thermal effects on spin transport along a deformable helical molecule in the presence of chiral-induced spin–orbit coupling. The carrier–lattice interaction is modeled by the well-established Peyrard–Bishop–Holstein model within the Langevin approach to include temperature as a stochastic noise. The carrier–lattice interaction causes the occurrence of polaron states in the molecule. We demonstrate the existence of two well-differentiated spin-dependent polaron transport regimes as a function of temperature. In the low-temperature regime, the spatial separation of the two spin-dependent polaron wave-packets results in a nonzero spin current. On the contrary, the spin current becomes negligible if the temperature of the system is high enough. Finally, we characterize this transition and estimate the critical temperature at which it takes place.

Solitons and polarons in organic helical molecules acquired a remarkable relevance after they were considered by Davydov to explain energy storage and transport in proteins.[1] They also play a fundamental role to understand denaturation during the DNA transcription according to the so-called Peyrard–Bishop (PBH) model.[2] In the last few decades, these models have widely been considered to analyze charge and energy transport properties of biological helical molecules.[3–9] The key point in all these descriptions is the major role that carrier–lattice interaction plays in organic molecules that have been demonstrated to be easily deformable.

More recently, a new intriguing phenomenon has attracted much attention to long-range carrier transport properties of helical and other chiral molecules, namely, the so-called chiral-induced spin selectivity (CISS). Indeed, there is a large variety of experimental evidence of spin-selective transport in chiral organic molecules.[10–22] To date, a number of theoretical models have been proposed to explain this phenomenon within different frameworks,[23–37] but none of them was able to successfully reproduce the large spin polarization observed in experiments. Therefore, this physical effect is still up for debate although there is a general agreement on the key ingredient that leads to CISS, namely, the influence of the helical spin–orbit coupling (SOC) and the exchange effects on the carrier dynamics derived from the helical conformation of the molecule. In the last few years, some studies have thoroughly investigated the carrier–lattice interaction impact on spin transport in organic helical molecules[38–44] and, in some cases, temperature effects have been considered as well.[44–46] This opened a new field of study where the propagation of spin-dependent polarons, as well as soliton solutions, is very relevant within the scope of non-linear quantum dynamics that we further explore in this work. Our results will be also relevant for other nonlinear physical systems where the influence of a helical SOC can be studied, i.e., Bose–Einstein condensates.[47–49]

In the following, we briefly introduce the non-linear model that describes spin transport in a deformable helical molecule. In addition to the unconventional Rashba-like SOC arising from its motion in the helical molecule, the carrier–lattice interaction is included by the way of the PBH model. Moreover, thermal effects are considered within the Langevin approach that makes necessary to use a special numerical algorithm to deal with stochastic Schrödinger equations. We then turn to the main goal of the work, namely, the detailed analysis of the spin-dependent wave-packet propagation and the resulting spin current along the system. As a major result, we find a crossover from coherent to incoherent spin-dependent transport on increasing temperature. Remarkably, the spin-dependent current displays a universal shape as a function of a reduced temperature, defined as the temperature scaled by the coupling constant of the underlying atomic lattice. This paves the way for an experimental validation of the model studying different helical molecules.

In order to provide an accurate description of the nucleotide dynamics and its effects on spin transport, our starting point is the PBH model.[2–6] In this model, the lattice dynamics is nonlinear, beyond the harmonic approximation, and it allows for a better description of large-amplitude vibrations of nucleotides. Notice that the most remarkable success of the PBH model is focused on the DNA denaturation occurring in the transcription process.[2,3]

The PBH Hamiltonian splits into three contributions

$$\mathscr{H} = \mathscr{H}_{\rm lat} + \mathscr{H}_{\rm e} + \mathscr{H}_{\rm int}. \tag{1}$$

The first term, $\mathscr{H}_{\rm lat}$, describes the lattice by mapping the double stranded DNA helix onto a one-dimensional (1D) lattice where every node represents a base pair.[2] Thus, a single degree of freedom y_n, representing the displacement from its equilibrium position, is assigned to every site. Under these considerations, $\mathscr{H}_{\rm lat}$ reads

$$\mathscr{H}_{\rm lat} = \sum_{n}^{N}\left[\frac{1}{2}m\dot{y}_n^2 + V(y_n) + W(y_n, y_{n-1})\right], \tag{2}$$

where m is the nucleotide mass and $n = 1, 2, \ldots, N$ labels the sites of the molecule.

Apart from the kinetic energy, there exist two other potential terms in Eq. (2): a local Morse potential $V(y_n)$ and a nonlinear stacking interaction potential $W(y_n, y_{n-1})$. They are defined as follows:

$$\begin{aligned} V_M(y_n) &= V_0\left(e^{-\alpha y_n} - 1\right)^2, \\ W(y_n, y_{n-1}) &= \frac{k}{4}\left(2 + e^{-\beta(y_n + y_{n-1})}\right)(y_n - y_{n-1})^2. \end{aligned} \tag{3}$$

The former takes into account the interactions within a DNA base pair as well as the repulsion between backbone phosphates and other surrounding solvent. The latter represents the nonlinear anharmonic coupling between nearest-neighbor nucleotides which gives rise to long-range interactions. Both potential terms depend on fitting parameters which were chosen to reproduce experimental DNA melting curves. Hereafter, we will use the following set of optimized parameters: $m = 300$ amu, $V_0 = 0.04$ eV, $\alpha = 4.45$ Å^{-1}, $k = 0.04$ eV/Å^2, and $\beta = 0.35$ Å$^{-1.3}$.

The carrier Hamiltonian, $\mathscr{H}_{\rm e}$, describes the spin transport along the helical molecule, as derived by Gutierrez *et al.*[26] It is worth mentioning that the latter agrees with the one proposed by Guo *et al.*[27] for the case of a pure radial helical electric field. In particular, we will consider a single strand and a single carrier level per site. The carrier Hamiltonian of the helical molecule reads

$$\mathscr{H}_{\rm e} = \sum_{n=1}^{N}\varepsilon_n c_n^\dagger c_n + \sum_{n=1}^{N-1}\left[c_n^\dagger \tau c_{n+1} + it_{\rm so}c_n^\dagger \alpha^n c_{n+1} + \text{H.c.}\right], \tag{4}$$

where $c_n^\dagger = (c_{n\uparrow}^\dagger, c_{n\downarrow}^\dagger)$ and $c_n = (c_{n\uparrow}, c_{n\downarrow})^{\mathsf{T}}$ are the creation and annihilation operators at site n of a helical molecule of length N. Here, the superscript T refers to the transpose and H.c. stands for the Hermitian conjugate. The on-site energies ε_n, the effective SOC constant $t_{\rm so}$, and the intersite hopping are considered within the matrix $\tau = \text{diag}(t_\uparrow, t_\downarrow)$ that will be assumed uniform along the molecule. The helical symmetry is included in the last term that is expressed as a function of the Pauli matrices, $\sigma_{x,y,z}$, such that $\alpha^n = (\sigma_n + \sigma_{n+1})$, being $\sigma_{n+1} = \sigma_z\cos\theta + \sin\theta[\sigma_x\sin(n\Delta\varphi) - \sigma_y\cos(n\Delta\varphi)]$, where θ is the helix angle and $\Delta\varphi$ refers to the twist angle between neighboring sites.[27] Hereafter, $\theta = 0.66$ rad and $\Delta\varphi = \pi/5$ rad will be considered as typical values for DNA molecules, corresponding to 10 sites per turn with a distance between consecutive sites of $\Delta z = 0.34$ nm. Figure 1 presents a planar view of a deformable helical molecule, indicating the various spin-dependent couplings between neighboring molecular sites. The last term in the Hamiltonian (1), $\mathscr{H}_{\rm int}$, takes into account the carrier–lattice interaction proposed by Holstein as an on-site energy correction as follows:[4]

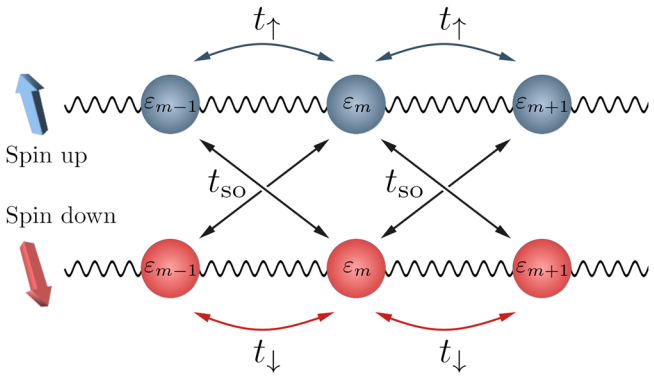

FIG. 1. Planar sketch of a deformable helical molecule. The parameters of the tight-binding Hamiltonian (4) and the carrier and the SOC between neighboring sites are shown.

$$\mathscr{H}_{\rm int} = \chi\sum_{n=1}^{N} y_n c_n^\dagger c_n. \tag{5}$$

Here, χ denotes the charge–lattice coupling constant that might depend on the sequence and the number of nucleotides.[50] It should be noted that *ab initio* estimations of this coupling χ are scarce, so in our simulations we will take a reference value to study its effects on the carrier dynamics as done in the previous works.

The equations of motion for the PBH model can be derived by treating the bases as classical oscillators, while the carrier is described quantum mechanically. This semiclassical approach is justified by the different time-scales of the charge and the lattice dynamics.[6] According to this formalism, the dynamics of the spinor components in the specific system of interest can be studied by the way of the following Schrödinger equations:

$$\begin{aligned} i\hbar\frac{d\psi_n^\uparrow}{dt} &= \varepsilon_n\psi_n^\uparrow + (t_\uparrow + it_{\rm so}\alpha_{1,1}^{n+1})\psi_{n+1}^\uparrow + (t_\uparrow - it_{\rm so}\alpha_{1,1}^{n-1})\psi_{n-1}^\uparrow \\ &\quad + it_{\rm so}\alpha_{1,2}^{n+1}\psi_{n+1}^\downarrow - it_{\rm so}\alpha_{1,2}^{n-1}\psi_{n-1}^\downarrow + \chi y_n\psi_n^\uparrow, \\ i\hbar\frac{d\psi_n^\downarrow}{dt} &= \varepsilon_n\psi_n^\downarrow + (t_\downarrow + it_{\rm so}\alpha_{2,2}^{n+1})\psi_{n+1}^\downarrow + (t_\downarrow - it_{\rm so}\alpha_{2,2}^{n-1})\psi_{n-1}^\downarrow \\ &\quad + it_{\rm so}\alpha_{2,1}^{n+1}\psi_{m+1}^\uparrow - it_{\rm so}\alpha_{2,1}^{n-1}\psi_{n-1}^\uparrow + \chi y_n\psi_n^\downarrow, \end{aligned} \tag{6}$$

where $\psi_n^\uparrow$ ($\psi_n^\downarrow$) is the probability amplitude of the charge carrier located at the nth base with spin up (down). The last term in Eq. (6) describes the carrier–lattice coupling through the constant χ and the displacement y_n of the nth nucleotide. Newton's equations of motion for the displacement y_n become

$$m\frac{d^2y_n}{dt^2} = -V_M'(y_n) - W'(y_n, y_{n-1}) - W'(y_n, y_{n+1}) - \chi|\psi_n|^2, \tag{7}$$

where the prime indicates differentiation with respect to y_n and $|\psi_n|^2 = |\psi_n^{\uparrow}|^2 + |\psi_n^{\downarrow}|^2$.

In order to include finite temperature effects on the spin transport, we consider the Langevin approach for the lattice dynamics. Therefore, we introduce two additional terms in Eq. (7) as follows:

$$m\frac{d^2y_n}{dt^2} = -V_M'(y_n) - W'(y_n, y_{n-1}) - W'(y_n, y_{n+1}) - \chi|\psi_n|^2 - m\gamma\frac{dy_n}{dt} + f_n(t)\,. \tag{8}$$

The force $f_n(t)$ describes the stochastic action of the environment due to thermal noise that is statistically balanced by the dissipative term that depends upon the parameter γ. In our simulations, we set $\gamma = 0.75\,\mathrm{fs}^{-1}$. According to the fluctuation–dissipation theorem, the following white-noise statistical properties hold:

$$\langle f_n(t)\rangle = 0, \qquad \langle f_n(t) f_n'(t')\rangle = 2\gamma m k_B T \delta_{nn'}\delta(t-t'), \tag{9}$$

where k_B is the Boltzmann constant and T is the temperature of the system. Such an approach is a microscopic model characterizing a water-type environment in terms of the collisions between the system and the fast reservoir molecules.[7,51] Due to the existence of stochastic terms in the lattice dynamics, a particular numerical approach is needed. In our simulations, we will use a suitable algorithm to integrate stochastic differential equations known as the $3_O4_S2_G$ procedure.[52,53]

In this work, we are interested in studying the propagation of a spin-dependent polaron along a helical molecule. Therefore, our starting point for all simulations will be an initially spin-unpolarized wave-packet in a lattice at equilibrium, so that $y_n(0) = 0$. As noticed in Ref. 39, in the absence of carrier–lattice interaction, the chiral-induced SOC may give rise to a spatial separation of the two spin-dependent components of the wave-packet. The propagation of both spins in opposite directions induces a finite spin current. In what follows, we will provide evidence that this trend remains only at low temperature. However, as we will demonstrate, such spin current is strongly temperature-dependent and we will focus on analyzing its behavior at a finite temperature.

For simplicity, hereafter, we will use spin-independent on-site energies $\varepsilon_n = 0.03\,\mathrm{eV}$ and intersite hopping $t_{\uparrow} = t_{\downarrow} \equiv t = 0.5\,\mathrm{eV}$. Moreover, our initial normalized wave-packet will be Gaussian such that $\psi_n^{\uparrow}(0) = \psi_n^{\downarrow}(0) \propto \exp[-(n-n_0)^2/w^2]$. All simulations were performed in a helical chain of size $N = 1500$, with initial parameters $n_0 = N/2$ and $w = 30$. Finally, since our focus of interest is the effect of finite temperature when there exists SOC, we will use a reference value of the charge–lattice coupling constant $\chi = 0.2\,\mathrm{eV/Å}$. Simulations with different values of χ within the range of 0.1–0.6 eV/Å have shown similar results. In order to assess the spin-transport properties of the helical molecule, we will monitor two related physical quantities. On the one hand, we will characterize the polaron propagation by means of the centroid $c(t)$ of both spin-dependent components of the wave-packet as follows:

$$c^{\sigma}(t) = \sum_{n=1}^{N} n|\psi_n^{\sigma}(t)|^2 - n_0, \tag{10}$$

with $\sigma = \uparrow, \downarrow$. On the other hand, and more relevant in the development of potential spintronic devices, we will calculate the resulting spin current with the following definition:[54]

$$J_s(t) = \frac{2\Delta z}{\hbar}\sum_{n=1}^{N}\mathrm{Im}\left[\hat{t}^*\psi_{n+1}^{\uparrow *}(t)\psi_n^{\uparrow}(t) - \hat{t}\psi_{n+1}^{\downarrow *}(t)\psi_n^{\downarrow}(t)\right]. \tag{11}$$

Here, we define $\hat{t} = t + 2it_{so}\cos(\theta)$.

In order to evaluate the stationary spin current when the temperature of the system is finite, a thermal average over time is required. Such average is performed by integrating the spin current for every time step, $J_s(t_i)$, over a period of time Δt. Averaging starts when the spin current has approximately reached its stationary value and finishes after a long enough time for which the dispersion of the mean value barely varies. Moreover, the small fluctuations at large times is taken as an estimation of the error bar for the spin current. Thus, the average spin current is characterized by the mean value as well as by the square root of the variance as follows:

$$\langle J_s\rangle = \frac{1}{N_t}\sum_{t_i\in\Delta t} J_s(t_i), \qquad \Delta J_s = \sqrt{\frac{1}{N_t}\sum_{t_i\in\Delta t}[J_s(t_i) - \langle J_s\rangle]^2}, \tag{12}$$

where N_t is the number of time steps in the simulations.

First, we analyze the dynamics of an initially spin-unpolarized polaron centered at the middle of the chain. Figure 2 shows the components of the carrier wave-function at time of $t = 400$ fs for different values of the temperature. The top panel displays the observed behavior of the spin-dependent polaron at $T = 0$, in agreement with the

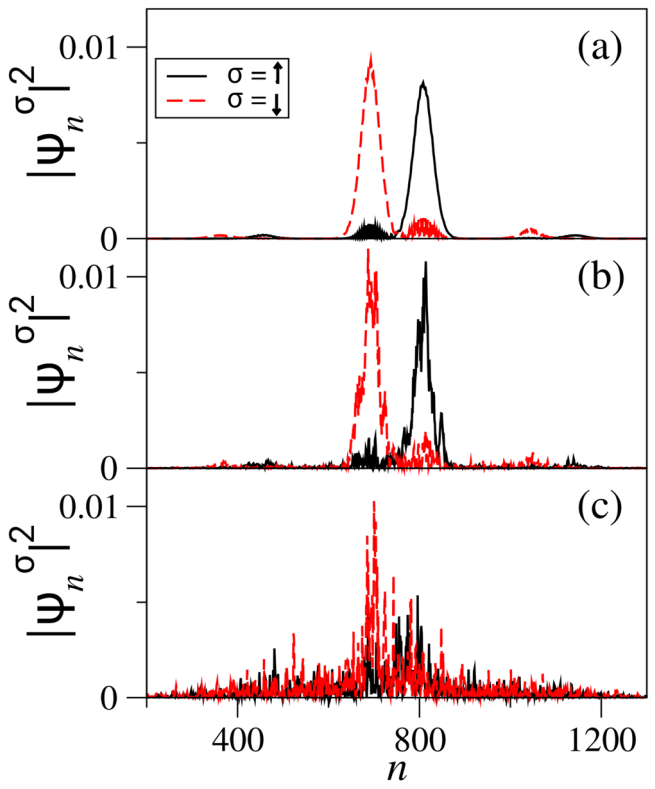

FIG. 2. Spin-dependent carrier wave-function at time $t = 400$ fs as a function of position in a lattice of $N = 1500$ sites with a SOC of $t_{so} = 0.03$ eV for different values of the system temperature (a) $T = 0$, (b) $T = 100$, and (c) $T = 200$ K.

results of Ref. 39. We observe a spatial separation of the two spin-components, signaling the appearance of a finite spin current. When the temperature reaches a value of $T = 100$ K, the wave-function still shows the same behavior, indicating the existence of a finite spin current across the molecule, as depicted in Fig. 2(b). However, on further increasing temperature up to $T = 200$ K, thermal noise spoils the coherence and the spatial separation of both components is almost unnoticeable, as shown in Fig. 2(c).

In order to get a better insight into the spatial propagation of the polaron, Fig. 3 presents the time-evolution of the centroid of every spin-component of the wave-function. Figure 3(a) shows the centroids as a function of time for different values of t_{so} and $T = 0$. As can be observed, the SOC is mainly responsible for the spin separation in the helical molecule. Indeed, such behavior disappears when $t_{so} = 0$ and becomes more relevant when t_{so} is increased. On the other hand, Fig. 3(b) shows the same magnitudes for a fixed $t_{so} = 0.03$ eV at different temperatures. These curves establish that thermal effects destroy coherence needed to spatially separate the two spin-components and, therefore, to give rise to a non-zero spin current, in agreement with Fig. 2. These results point out the existence of a transition with regard to the spin transport as a function of temperature. For the particular parameters considered in the simulations shown in Fig. 3, such a transition takes place at a temperature between $T = 100$ and $T = 200$ K.

We now discuss the spin current, defined in Eq. (11), resulting from the separation of both spin components. As we are mainly interested in the temperature of the transition of the spin current, we will present it in arbitrary units. Figure 4 shows the time-dependent spin current for several values of temperature. In all considered cases but the case at $T = 0$, one can see how thermal effects gives rise to a noisy spin current that, for long enough times ($t > 200$ s), reaches a plateau. In Fig. 4, we provide additional evidence of the existence of the thermal transition occurring within the temperature range $100 - 200$ K. For $T < 100$ K, the obtained spin current is quite steady around a clear non-zero value. However, if $T > 200$ K, the spin current rapidly evolves to zero, although its fluctuations around this value increase with temperature. In view of these results, we can conclude that two well differentiated regimes for long-range spin transport exist in the helical molecule when temperature changes.

Once the thermal transition in the system has clearly been established, this section is devoted to its characterization. In order to do that, we focus now on the thermal average of the spin current as explained before. It is worth noticing that in our model thermal effects are included by the way of the lattice dynamics represented in Eq. (8) so that any thermal effect comes from the phonon bath. In view of the lattice potentials given by Eq. (3), it is clear that the most relevant parameter for the phonon dynamics is the lattice constant k. Therefore, the transition temperature between the two spin-transport regimes needs to be related to k.

Figure 5(a) shows the average spin current as a function of the temperature of the system for several values of the lattice constant around the PBH value ($k = 0.04$ eV/Å^2). In all considered cases, a

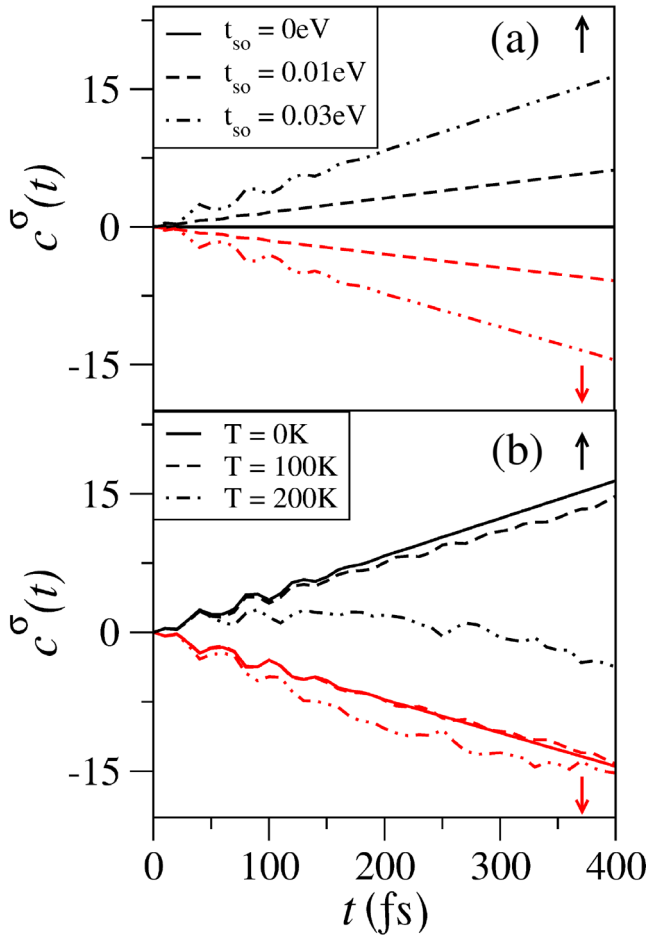

FIG. 3. Centroid of the spin-dependent carrier wave-function in a lattice of $N = 1500$ sites for (a) different values of the SOC at $T = 0$ and (b) different temperatures but a fixed $t_{so} = 0.03$ eV.

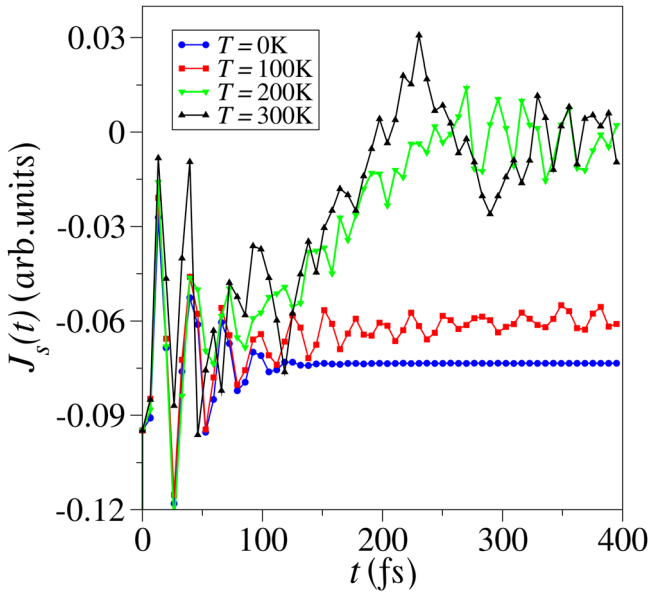

FIG. 4. Time-evolution of the spin current during thermalization in a chain of $N = 1500$ sites for different values of the system temperature.

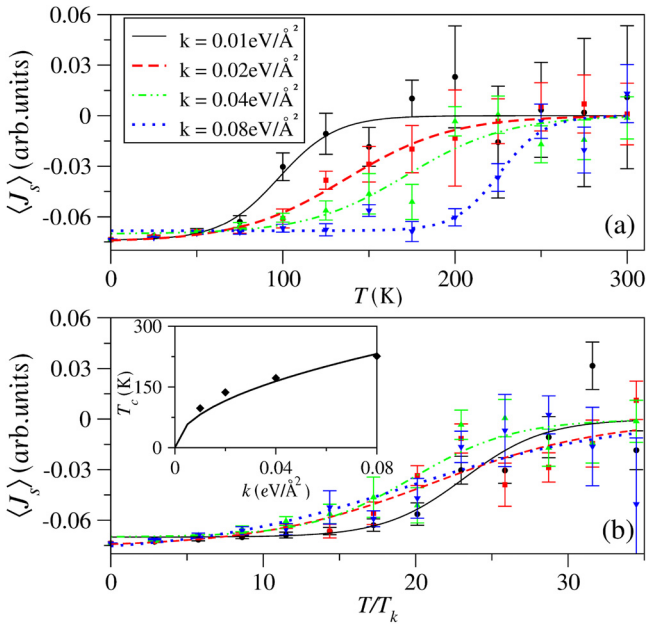

FIG. 5. Thermalized spin current for different values of the stacking potential parameter k as a function of (a) temperature T and (b) the reduced temperature $T/\sqrt{k}$. Inset shows the transition temperature as a function of k. Symbols refer to fitting values in comparison with the solid line $\sqrt{k}$.

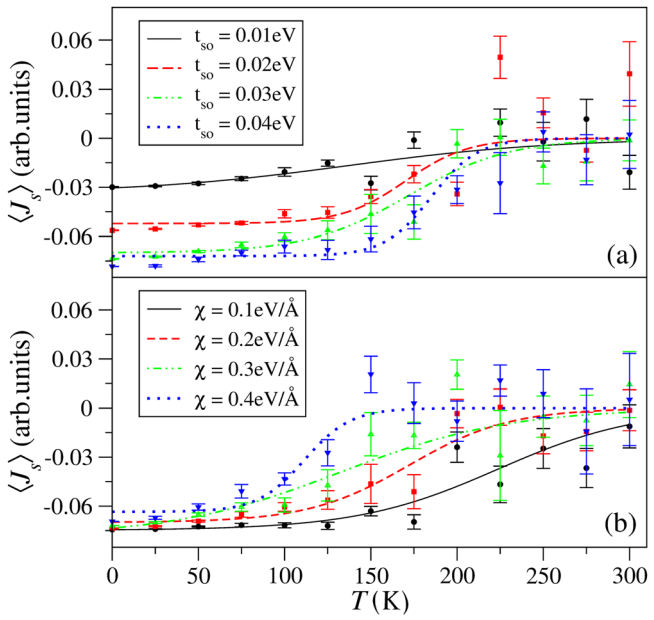

FIG. 6. Thermalized spin current for different values of the spin–orbit t_{so} and charge–lattice χ couplings as a function of temperature T.

smooth thermal transition is clearly established. Dispersion of the data is almost negligible at low temperature when the spin current reaches a well-defined non-zero value. However, they increase as the temperature rises up to the thermal transition to get the largest values when the spin current presents strong fluctuations around zero (see Fig. 4). Figure 5(a) also reveals that the thermal transition is shifted to higher temperatures when the lattice-constant is increased. The latter can be roughly understood by considering a 1D harmonic lattice. In such a case, the phonon bandwidth is $\Delta = \hbar\sqrt{4k/m}$. The latter must be compared to the energy associated with the thermal vibrations in order to separate the two spin-transport regimes. Thus, if $\Delta \gg k_B T$, the system will be in the low-temperature regime and vice versa. This means that the critical temperature will be then smaller if the lattice constant is reduced. This is consistent with the results shown in Fig. 5(a). Figure 5(b) provides further support to the previous reasoning. Here, the spin current is represented as a function of a reduced temperature $T/\sqrt{k}$ so that the dependence on the phonon bandwidth is removed. As expected, the transition of the spin current now occurs for the same reduced temperature, independently of the considered lattice constant. Finally, we obtain the value of the critical temperature by fitting the spin current shown in Fig. 5(a) to the function $F(T) \propto 1 - \tanh[(T - T_c)/a]$. The inset of Fig. 5(b) represents the obtained critical values on top of the curve $T(k) = \sqrt{k}$, showing a really good agreement. Once more, this supports our understanding of the thermal transition in regard to the phonon dynamics in the molecule.

Finally, we analyze how these results will be affected by the change in the most characteristic parameters of the model, namely, the spin–orbit coupling and the charge–lattice interaction. Figures 6(a) and 6(b) present the average spin-current as a function of the temperature for the case of reference considered in Fig. 4 but different values of t_{so} or χ, respectively. In all considered cases, the thermal transition is still clearly present. Nevertheless, the magnitude of the low-temperature spin-current and the transition temperature T_c depend on the particular values of the model parameters. Figure 6(a) shows that the nonzero spin-current is strongly reduced if the spin–orbit coupling in the system decreases. This was already pointed out in Fig. 3(a). However, it turns out that such spin-current saturates for a large enough t_{so} and hardly depends on the charge–lattice coupling [see Fig. 6(b)]. On the other hand, an increase in χ or a decrease in t_{so}, although to a lower extend, gives rise to a shift of the transition temperature to lower value. This will lead eventually to a reduction in the thermal operating window of the spin transport in the system.

In this paper, we have proposed a formalism to include thermal effects in the long-range spin transport in helical molecules. Our proposal is to combine two different approaches already demonstrated as powerful tools to describe carrier dynamics in DNA molecules. On the one hand, the carrier dynamics is described by way of a tight-binding Hamiltonian already established to describe the chiral-induced spin–orbit coupling in helical molecules.[26,27] On the other hand, the carrier–lattice coupling, in addition to the effect of temperature, is modeled by means of the PBH model combined with the Langevin approach.[2,7] The consideration of this thermal noise needs a particular numerical algorithm to integrate stochastic differential equations.[52,53]

We characterize the time-evolution of an initially spin-unpolarized spinor wave-packet located in the lattice in its equilibrium configuration. We establish that there exists a thermal transition between two well-differentiated regimes. At temperatures below a critical one, our results demonstrate that, due to the chiral-induced spin–orbit coupling, the wave-packets associated with both spinor

components propagate in opposite directions. This is a clear evidence of the existence of a nonzero spin current. Such a behavior is consistent with a previous study at $T = 0$, in which no carrier–lattice interaction was considered.[39] However, if the temperature of the system is larger than the critical one, this remarkable feature disappears since the spinor wave-packet spreads out very quickly and no net spin separation can be observed. Therefore, the resulting spin current oscillates around zero due to the thermal fluctuations. Lowering the charge– carrier and spin–orbit coupling constants below the values widely used in the literature results in a slight decrease in the transition temperature, but the general trend of the phenomenon remains. Finally, we discuss this thermal transition and calculate the critical temperature in comparison with the phonon dynamics of the PBH lattice.[2] Here, we take as a reference scenario a 1D harmonic lattice to estimate that the critical temperature scales with the stacking constant as $\sqrt{k}$. We numerically demonstrate that in the system under consideration, although it is clearly more complex than the 1D harmonic lattice [see Eq. (8)], such a trend still holds.

It is worth mentioning that the charge transport in DNA molecules has been proved to be clearly affected by disorder correlations due to dynamical fluctuations from the surrounding solvent.[55] Although a detailed study of this issue is beyond the present study, let us briefly discuss this regard. Indeed, such effects result in a widening of the system transmission band which can be effectively considered as an increase in its electronic hopping. In Ref. 56, it was also demonstrated that the effective hopping increases with lowering the temperature in molecular nanowires. Therefore, the eventual inclusion of on-site disorder correlations in our model would lead to a lower effective temperature in our simulations. Thus, the transition temperature at which the system stops supporting a non-zero spin-current will be higher and a larger thermal operating region for our proposed device would be expected.

The authors thank R. P. A. Lima for helpful discussions. This research has been supported by Ministerio de Ciencia e Innovación (Grant No. PID2019-106820RB-C21).

AUTHOR DECLARATIONS

Conflict of Interest

The authors have no conflicts to disclose.

Author Contributions

Miguel Barroso: Investigation (equal). **José Balduque:** Investigation (equal). **Francisco Dominguez-Adame:** Funding acquisition (equal); Investigation (equal). **Elena Diaz Garcia:** Funding acquisition (equal); Investigation (lead).

DATA AVAILABILITY

The data that support the findings of this study are available from the corresponding author upon reasonable request.

REFERENCES

[1]A. S. Davydov, "Solitons in molecular systems," Phys. Scr. **20**, 387 (1979).
[2]M. Peyrard and A. R. Bishop, "Statistical mechanics of a nonlinear model for DNA denaturation," Phys. Rev. Lett. **62**, 2755 (1989).
[3]T. Dauxois, M. Peyrard, and A. R. Bishop, "Entropy-driven DNA denaturation," Phys. Rev. E **47**, R44–R47 (1993).
[4]S. Komineas, G. Kalosakas, and A. Bishop, "Effects of intrinsic base-pair fluctuations on charge transport in DNA," Phys. Rev. E **65**, 061905 (2002).
[5]P. Maniadis, G. Kalosakas, K. O. Rasmussen, and A. R. Bishop, "Ac conductivity in a DNA charge transport model," Phys. Rev. E **72**, 021912 (2005).
[6]G. Kalosakas, S. Aubry, and G. P. Tsironis, "Polaron solutions and normal-mode analysis in the semiclassical Holstein model," Phys. Rev. B **58**, 3094–3104 (1998).
[7]G. Kalosakas, K. O. Rasmussen, and A. R. Bishop, "Charge trapping in DNA due to intrinsic vibrational hot spots," J. Chem. Phys. **118**, 3731 (2003).
[8]L. Cruzeiro, "The Davydov/Scott model for energy storage and transport in proteins," J. Biol. Phys. **35**, 43–55 (2009).
[9]E. Díaz, R. P. A. Lima, and F. Domínguez-Adame, "Bloch-like oscillations in the Peyrard-Bishop-Holstein model," Phys. Rev. B **78**, 134303 (2008).
[10]B. Göhler, V. Hamelbeck, T. Z. Markus, M. Kettner, G. F. Hanne, Z. Vager, R. Naaman, and H. Zacharias, "Spin selectivity in electron transmission through self-assembled monolayers of double-stranded DNA," Science **331**, 894 (2011).
[11]Z. Xie, T. Z. Markus, S. R. Cohen, Z. Vager, R. Gutiérrez, and R. Naaman, "Spin specific electron conduction through DNA oligomers," Nano Lett. **11**, 4652 (2011).
[12]D. Mishra, T. Z. Markus, M. Naaman, R. Kettner, B. Gohler, H. Zacharias, N. Friedman, M. Sheves, and C. Fontanesi, "Spin-dependent electron transmission through bacteriorhodopsin embedded in purple membrane," Proc. Natl. Acad. Sci. U. S. A. **110**, 14872 (2013).
[13]O. B. Dor, S. Yochelis, S. P. Mathew, R. Naaman, and Y. Paltiel, "A chiral-based magnetic memory device without a permanent magnet," Nat. Commun. **4**, 2256 (2013).
[14]M. Kettner, B. Göhler, H. Zacharias, D. Mishra, V. Kiran, R. Naaman, C. Fontanesi, D. H. Waldeck, S. Sęk, J. Pawłowski, and J. Juhaniewicz, "Spin filtering in electron transport through chiral oligopeptides," J. Phys. Chem. C **119**, 14542 (2015).
[15]P. C. Mondal, C. Fontanesi, D. H. Waldeck, and R. Naaman, "Field and chirality effects on electrochemical charge transfer rates: Spin dependent electrochemistry," ACS Nano **9**, 3377 (2015).
[16]H. Einati, D. Mishra, N. Friedman, M. Sheves, and R. Naaman, "Light-controlled spin filtering in bacteriorhodopsin," Nano Lett. **15**, 1052 (2015).
[17]V. Kiran, S. P. Mathew, S. R. Cohen, I. Hernández Delgado, J. Lacour, and R. Naaman, "Helicenes–A new class of organic spin filter," Adv. Mater. **28**, 1957 (2016).
[18]A. C. Aragonès, E. Medina, M. Ferrer-Huerta, N. Gimeno, M. Teixidó, J. L. Palma, N. Tao, J. M. Ugalde, E. Giralt, I. Díez-Pérez, and V. Mujica, "Measuring the spin-polarization power of a single chiral molecule," Small **13**, 1602519 (2017).
[19]V. Kiran, S. R. Cohen, and R. Naaman, "Structure dependent spin selectivity in electron transport through oligopeptides," J. Chem. Phys. **146**, 92302 (2017).
[20]A. Kumar, E. Capua, M. K. Kesharwani, J. M. L. Martin, E. Sitbon, D. H. Waldeck, and R. Naaman, "Chirality-induced spin polarization places symmetry constraints on biomolecular interactions," Proc. Natl. Acad. Sci. U. S. A. **114**, 2474 (2017).
[21]O. Ben Dor, S. Yochelis, A. Radko, K. Vankayala, E. Capua, A. Capua, S.-H. Yang, L. T. Baczewski, S. S. P. Parkin, R. Naaman, and Y. Paltiel, "Magnetization switching in ferromagnets by adsorbed chiral molecules without current or external magnetic field," Nat. Commun. **8**, 14567 (2017).
[22]M. Kettner, V. V. Maslyuk, D. Nürenberg, J. Seibel, R. Gutierrez, G. Cuniberti, K.-H. Ernst, and H. Zacharias, "Chirality-dependent electron spin filtering by molecular monolayers of helicenes," J. Phys. Chem. Lett. **9**, 2025 (2018).
[23]S. Yeganeh, M. A. Ratner, E. Medina, and V. Mujica, "Chiral electron transport: Scattering through helical potentials," J. Chem. Phys. **131**, 014707 (2009).
[24]E. Medina, F. López, M. A. Ratner, and V. Mujica, "Chiral molecular films as electron polarizers and polarization modulators," Europhys. Lett. **99**, 17006 (2012).
[25]R. Gutiérrez, E. Díaz, R. Naaman, and G. Cuniberti, "Spin-selective transport through helical molecular systems," Phys. Rev. B **85**, 081404 (2012).
[26]R. Gutierrez, E. Diaz, C. Gaul, T. Brumme, F. Domínguez-Adame, and G. Cuniberti, "Modeling spin transport in helical fields: Derivation of an effective low-dimensional Hamiltonian," J. Phys. Chem. C **117**, 22276 (2013).
[27]A.-M. Guo and Q.-F. Sun, "Spin-selective transport of electrons in DNA double helix," Phys. Rev. Lett. **108**, 218102 (2012).

[28]A. A. Eremko and V. M. Loktev, "Spin sensitive electron transmission through helical potentials," Phys. Rev. B **88**, 165409 (2013).
[29]D. Rai and M. Galperin, "Electrically driven spin currents in DNA," J. Phys. Chem. C **117**, 13730 (2013).
[30]E. Medina, L. A. González-Arraga, D. Finkelstein-Shapiro, B. Berche, and V. Mujica, "Continuum model for chiral induced spin selectivity in helical molecules," J. Chem. Phys. **142**, 194308 (2015).
[31]K. Michaeli, V. Varade, R. Naaman, and D. H. Waldeck, "A new approach towards spintronics–spintronics with no magnets," J. Phys.: Condens. Matter **29**, 103002 (2017).
[32]S. Matityahu, Y. Utsumi, A. Aharony, O. Entin-Wohlman, and C. A. Balseiro, "Spin-dependent transport through a chiral molecule in the presence of spin-orbit interaction and nonunitary effects," Phys. Rev. B **93**, 075407 (2016).
[33]V. V. Maslyuk, R. Gutierrez, A. Dianat, V. Mujica, and G. Cuniberti, "Enhanced magnetoresistance in chiral molecular junctions," J. Phys. Chem. Lett. **9**, 5453 (2018).
[34]J. Fransson, "Chirality-induced spin selectivity: The role of electron correlations," J. Phys. Chem. Lett. **10**, 7126 (2019).
[35]A. Ghazaryan, M. Lemeshko, and A. G. Volosniev, "Filtering spins by scattering from a lattice of point magnets," Commun Phys **3**, 178 (2020).
[36]A. Shitade and E. Minamitani, "Geometric spin–orbit coupling and chirality-induced spin selectivity," New J. Phys. **22**, 113023 (2020).
[37]S. Alwan and Y. Dubi, "Spinterface origin for the chirality-induced spin-selectivity effect," J. Am. Chem. Soc. **143**, 14235 (2021).
[38]S. Behnia, S. Fathizadeh, and A. Akhshani, "DNA spintronics: Charge and spin dynamics in DNA wires," J. Phys. Chem. C **120**, 2973 (2016).
[39]R. A. Caetano, "Spin-current and spin-splitting in helicoidal molecules due to spin-orbit coupling," Sci. Rep. **6**, 23452 (2016).
[40]S. V. Salazar, V. Mujica, and E. Medina, "Spin-orbit coupling modulation in DNA by mechanical deformations," Chimia **72**, 411 (2018).
[41]P. Albares, E. Díaz, J. M. Cerveró, F. Domínguez-Adame, E. Diez, and P. G. Estevez, "Spin dynamics in helical molecules with non-linear interactions," Phys. Rev. E **97**, 022210 (2018).
[42]T. Gao, Q. Tian, M. Du, L. Zhang, X. Liu, W. Qin, and S. Xie, "Synergistic effect of carrier velocity and density on chirality-induced spin selectivity in helical organic devices," Appl. Phys. Lett. **120**, 032405 (2022).
[43]G.-F. Du, H.-H. Fu, and R. R. Wu, "Vibration-enhanced spin-selective transport of electrons in the DNA double helix," Phys. Rev. B **102**, 035431 (2020).
[44]E. Díaz, F. Domínguez-Adame, R. Gutierrez, G. Cuniberti, and V. Mujica, "Thermal decoherence and disorder effects on chiral-induced spin selectivity," J. Phys. Chem. Lett. **9**, 5753 (2018).
[45]Y. Sang, S. Mishra, F. Tassinari, S. K. Karuppannan, R. Carmieli, R. D. Teo, A. Migliore, D. N. Beratan, H. B. Gray, I. Pecht, J. Fransson, D. H. Waldeck, and R. Naaman, "Temperature dependence of charge and spin transfer in azurin," J. Phys. Chem. C **125**, 9875 (2021).
[46]T. K. Das, F. Tassinari, R. Naaman, and J. Fransson, "Temperature-dependent chiral-induced spin selectivity effect: Experiments and theory," J. Phys. Chem. C **126**, 3257–3264 (2022).
[47]Y.-J. Lin, K. Jiménez-García, and I. B. Spielman, "Spin-orbit-coupled Bose-Einstein condensates," Nature **471**, 83 (2011).
[48]V. Achilleos, D. J. Frantzeskakis, P. G. Kevrekidis, and D. E. Pelinovsky, "Matter-wave bright solitons in spin-orbit coupled Bose-Einstein condensates," Phys. Rev. Lett. **110**, 264101 (2013).
[49]Y. V. Kartashov and V. V. Konotop, "Solitons in Bose-Einstein condensates with helicoidal spin-orbit coupling," Phys. Rev. Lett. **118**, 190401 (2017).
[50]J. A. Berashevich, V. Apalkov, and T. Chakraborty, "Polaron tunneling dynamics of a linear polymer of nucleotides," J. Phys.: Condens. Matter **20**, 075104 (2008).
[51]C. Gardiner, *Stochastic Methods; A Handbook for the Natural and Social Sciences*, (Springer Berlin, Heidelberg, 2009), Edition No. 4, p XVIII; available at https://link.springer.com/book/9783540707127.
[52]E. Helfand, "Numerical integration of stochastic differential equations," Bell Syst. Tech. J. **58**, 2289 (1979).
[53]H. S. Greenside and E. Helfand, "Numerical integration of stochastic differential equations—II," Bell Syst. Tech. J. **60**, 1927 (1981).
[54]J. Shi, P. Zhang, D. Xiao, and Q. Niu, "Proper definition of spin current in spin-orbit coupled systems," Phys. Rev. Lett. **96**, 076604 (2006).
[55]R. Gutiérrez, R. Caetano, P. B. Woiczikowski, T. Kubar, M. Elstner, and G. Cuniberti, "Structural fluctuations and quantum transport through DNA molecular wires: A combined molecular dynamics and model Hamiltonian approach," New J. Phys. **12**, 023022 (2010).
[56]P. Thiessen, E. Díaz, R. A. Römer, and F. Domínguez-Adame, "Nonequilibrium transport through a disordered molecular nanowire," Phys. Rev. B **95**, 195431 (2017).